Chemistry–A European Journal

Supporting Information

Luminescent Chiral Exciplexes with Sky-Blue and Green Circularly Polarized-Thermally Activated Delayed Fluorescence

Chemistry–A European Journal

Supporting Information

Luminescent Chiral Exciplexes with Sky-Blue and Green Circularly Polarized-Thermally Activated Delayed Fluorescence

Supporting Information

Table of Contents

A. General methods

^{1}H and ^{13}C NMR spectra were recorded at room temperature on an *AVANCE III 400 BRUKER* at the Centre Régional de Mesures Physiques de l'Ouest (CRMPO), Université de Rennes 1. Chemical shifts δ are given in ppm and coupling constants *J* in Hz. Chemical shifts for ^{1}H NMR spectra are referenced relative to residual protium in the deuterated solvent (δ = 7.26 ppm, $CDCl_3$). ^{13}C shifts are referenced to $CDCl_3$ peaks at δ = 77.16 ppm.

High-resolution mass (HR-MS) determinations were performed at CRMPO on a Bruker MaXis 4G by ESI and MALDI with CH_2Cl_2 as solvent techniques. Experimental and calculated masses are given with consideration of the mass of the electron.

UV-Visible (UV-vis, in M^{-1} cm^{-1}) absorption spectra were recorded on a UV-2401PC Shimadzu spectrophotometer.

Steady-state luminescence spectra were measured using an Edinburgh FS920 Steady State Fluorimeter combined with a FL920 Fluorescence Lifetime Spectrometer. The spectra were corrected for the wavelength dependence of the detector, and the quoted emission maxima refer to the values after correction. Life-times measurements were conducted with 375 nm diode laser excitation (EPL-series) plugged to a TCSPC pulsed source interface. Absolute fluorescence quantum yields ϕ were recorded with a Hamamatsu C9920-03 integrating sphere.

Electrochemical measurements were performed with a potentiostat-galvanostat AutoLab PGSTAT 302N controlled by resident GPES (General Purpose Electrochemical System 4.9) software using a conventional single-compartment three-electrode cell. The working and auxiliary electrodes were platinum electrodes and the reference electrode were the saturated potassium chloride calomel electrode (SCE). The supporting electrolyte was 0.2 N Bu_4NPF_6 (tetrabutylammonium hexafluorophosphate) in dichloromethane and solutions were purged with argon before the measurements. All potentials are quoted relative to SCE, and the scan rate was either 100 or 200 mV/s.

The thin films used in this study have been prepared on glass substrates by spin coating solutions of either the pure donor compound, or a mixture of the donor and acceptor molecules in the indicated weight ratio, all being at a concentration of ~ 10 $mg.mL^{-1}$. 0.1 mL of the solution is deposited on the glass fixed within the spin-coater holder, and the film is obtained using a sequence including 60 seconds of rotation, with an acceleration of 500 $rpm.s^{-1}$ and a maximum speed of 2000 rpm.

For the vacuum luminescence measurement, a piece of the glass substrate was placed in a nmr tube with a J. Young valve, which can be freed from oxygen with a residual pressure of ~10^{-2} mbar. Then the tube can be placed in a dedicated holder for fluorescence measurements.

Electronic circular dichroism (ECD, in M^{-1} cm^{-1}) was measured on a Jasco J-815 Circular Dichroism Spectrometer (IFR140 facility - Biosit - Université de Rennes 1). Specific rotations (in deg cm^2 g^{-1}) were measured in a 0.2 cm thermostated quartz cell on a PerkinElmer Model 341 polarimeter.

The circularly polarized luminescence (CPL) measurements were performed using a home-built CPL spectrofluoropolarimeter (constructed with the help of the JASCO Company). The samples were excited using a 90° geometry with a Xenon ozone-free lamp 150 W LS. The following parameters were used: emission slit width ≈ 2 mm, integration time = 4 sec, scan speed = 50 nm/min, accumulations = 10. The concentration of all the samples was ca. 10^{-5} M.

Enantiomers of 2 were separated using chiral preparative SFC (Jasco SFC-4000) using the conditions indicated in page S17. Thin-layer chromatography (TLC) was performed on aluminum sheets precoated with Merck 5735 Kieselgel 60F254. Column chromatography was carried out with Merck 5735 Kieselgel 60F (0.040-0.063 mm mesh). Chemicals were purchased from Sigma-Aldrich, Alfa Aesar or TCI Europe and used as received.

B. Synthetic procedures

1 was synthesized according to previous synthetic procedures.[1]

2 was synthesized via iodination reaction of **1** with NIS in a mixture of $CHCl_3/CH_3COOH$ at 0°C, and followed by a Suzuki coupling reaction with 2-cyanophenylboronic acid in a mixture of DMF/H_2O in the presence of $Pd(PPh_3)_4$ as a catalyst and K_2CO_3 as base.

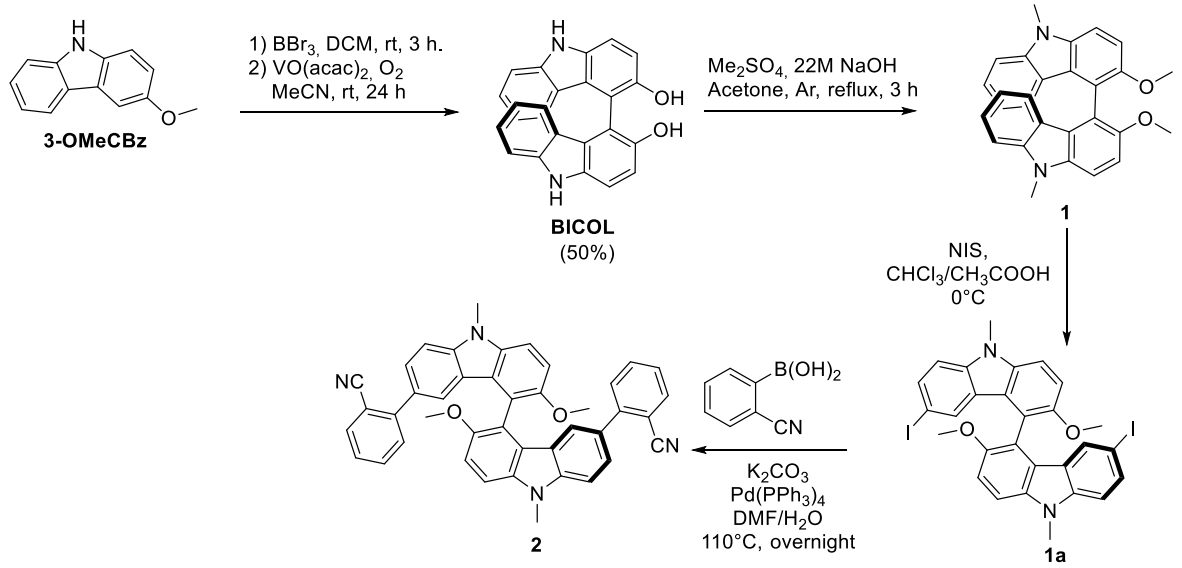

Scheme S1. BICOL, **1** and **2** derivatives synthesis.

(±)-2,2'-(3,3'-dimethoxy-9,9'-dimethyl-9H,9'H-[4,4'-bicarbazole]-6,6'-diyl)dibenzonitrile (**2**)

In a round bottom flask, 200 mg (0.48 mmol) of **1** was dissolved in 6 ml of $CHCl_3$ and 3 ml of CH_3COOH, then N-iodosuccinimide 193 mg (0.86 mmol) was slowly added. The reaction was stirred at 0 ℃ for 20 minutes, followed bt TLC. The mixture was then poured into 20 mL dichloromethane and washed with sat. $Na_2S_2O_3$ solution (20 mL), water (2 x 30 mL) and brine (1 x 30 mL). The organic phase was dried over $MgSO_4$ and the solvents evaporated under reduce pressure. The crude product was passed through a short silica plug ($CHCl_3$) to yield **1a** (280 mg, 87 %) as off white solid. The product was directly used without futher purification.
In a pre-dried schlenk flask, 81 mg (0.12 mmol) of **1a**, 107 mg (0.72 mmol) of 2-cyanophenylboronic acid, 31 mg (0.80 mmol) of K_2CO_3 and 23 mg (0.02 mmol) of $Pd(PPh_3)_4$ were disolved in 16 mL of a mixture of DMF/H_2O. The reaction was refluxed under argon over night, and then poured into 20 mL of dichloromethane and washed with water (2 x 30 mL) and brine (1 x 30 mL). The organic phase was dried over $MgSO_4$ and the solvents evaporated under reduce pressure. The crude product was passed through a short silica plug (EtOAC : heptane 1:2) to yield **2** (30 mg, 40 %).

^{1}H NMR (400 MHz, Methylene Chloride-d_2) δ 7.65 (dd, *J* = 7.7, 1.4 Hz, 2H), 7.60 – 7.49 (m, 6H), 7.53 – 7.45 (m, 4H), 7.48 – 7.40 (m, 4H), 7.39 – 7.28 (m, 5H), 7.02 (dd, *J* = 7.8, 1.1 Hz, 2H), 6.73 (d, *J* = 1.8 Hz, 2H), 3.93 (s, 6H), 3.80 (s, 6H).

^{13}C NMR (400 MHz, Methylene Chloride-d_2) δ 151.1, 146.2, 142.0, 137.3, 133.5, 132.2, 130.0, 128.0, 126.3, 126.3, 122.8, 122.0, 122.0, 119.7, 118.7, 112.2, 110.8, 108.3, 108.1, 57.3, 29.2.

HR-MS Thermo-Fisher Q-Exactive, ESI (+), CH_3OH/CH_2Cl_2 (90/10); ion $[M+Na]^+$, $C_{42}H_{30}N_4O_2Na$, m/z calculated 645.2261, m/z experimental 645.2263 (Δ=0 ppm).

Experimental optical rotation values

(+)-**2**: $[\alpha]_D^{25}$ = +392 deg cm^2 g^{-1} ± 10%, $[\phi]_D^{25}$ = +2441 deg cm^2 mol^{-1} (c = 1.3 × 10^{-3} , $CHCl_3$).
(-)-**2**: $[\alpha]_D^{25}$ = -385 deg cm^2 g^{-1} ± 10%, $[\phi]_D^{25}$ = –2397 deg cm^2 mol^{-1} (c = 1.2 × 10^{-3}, $CHCl_3$).

C. Steady-state photophysical and chiroptical characterizations

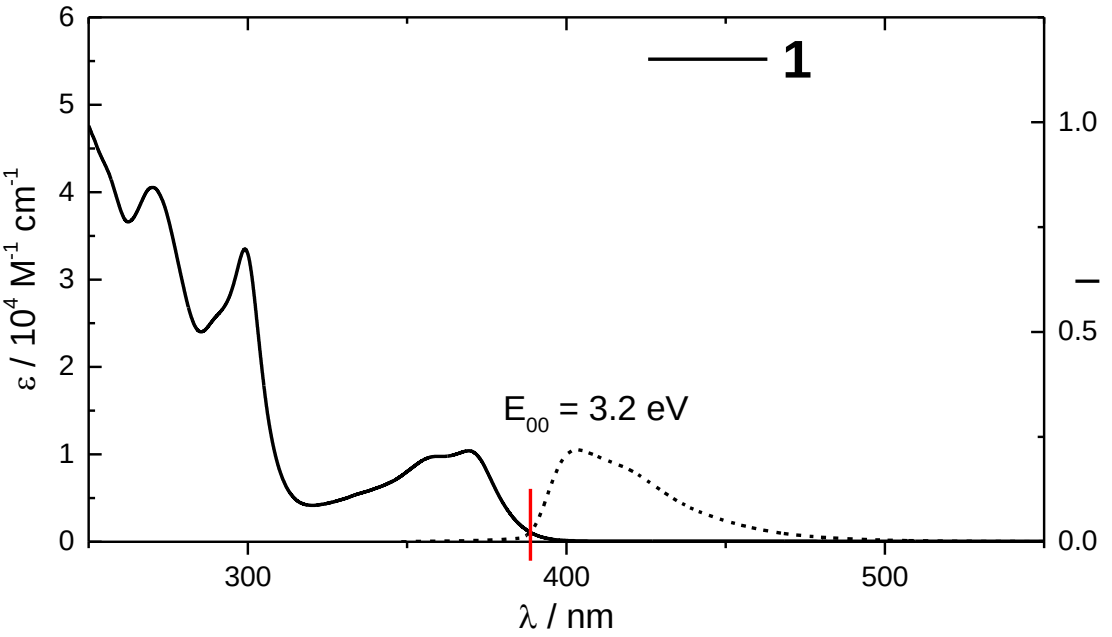

Figure S1. UV-vis (solid line) and fluorescence spectra (dash line) of compound **1** (black) in dichloromethane (*ca.* 10^{-5} M) at 298 K.

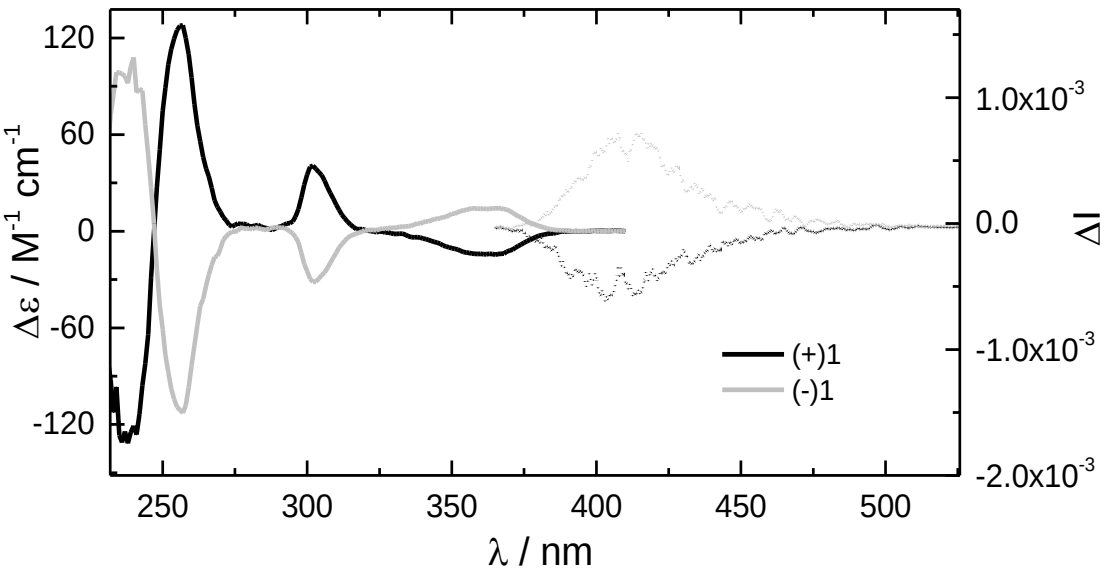

Figure S2. Electronic circular dichroism (ECD) spectra of enantiopure (+)-/(-)-**1** and corresponding mirror-image CPL spectra measured in dichloromethane (*ca.* 10^{-5} M) at 298 K, enabling us to determine a g_{lum} factor of 0.7 × 10^{-3} for **1**

a)

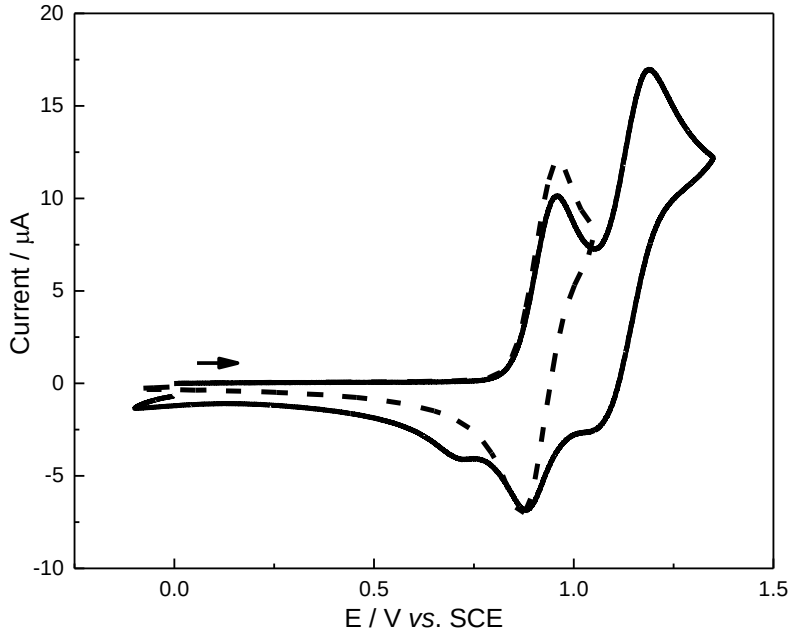

b)

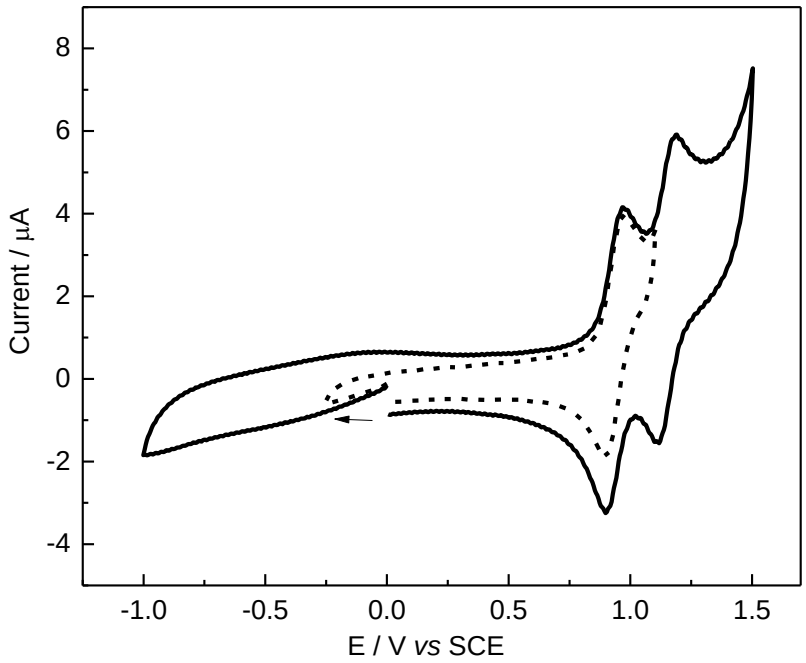

Figure S3. Cyclic voltammograms of a) **1** and b) **2** *versus* saturated calomel electrode (SCE) as the reference and 0.2 M Bu_4NPF_6 in CH_2Cl_2 with a scan rate of 200 mV/s.

Table S1. Oxidation potentials ($E_{1/2}^{ox}$ in V) of **1**, **2**, calculated from their respective anodic and cathodic peaks, and recorded *versus* saturated calomel electrode (SCE).

Compound	$E_{1/2}^{ox1}$	$E_{1/2}^{ox2}$
1	+0.92	+1.11
2	+0.93	+1.15

D. Exciplex Characterizations

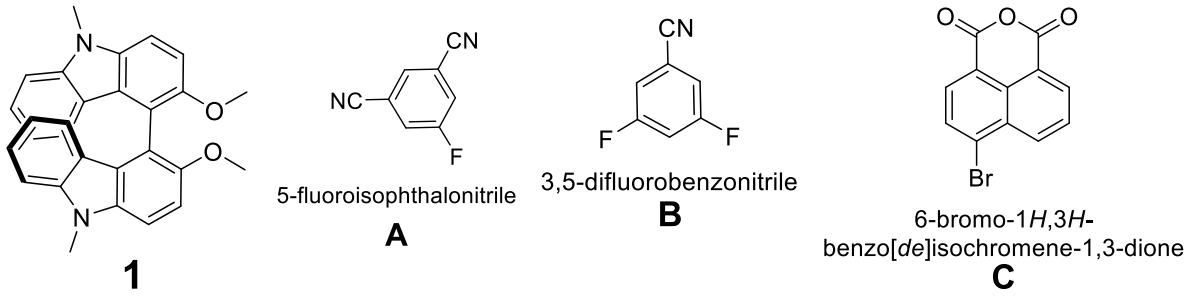

Figure S4. Chemical structures of the chiral electron donor **1** and the electron acceptors used in this study, as received from chemical suppliers.

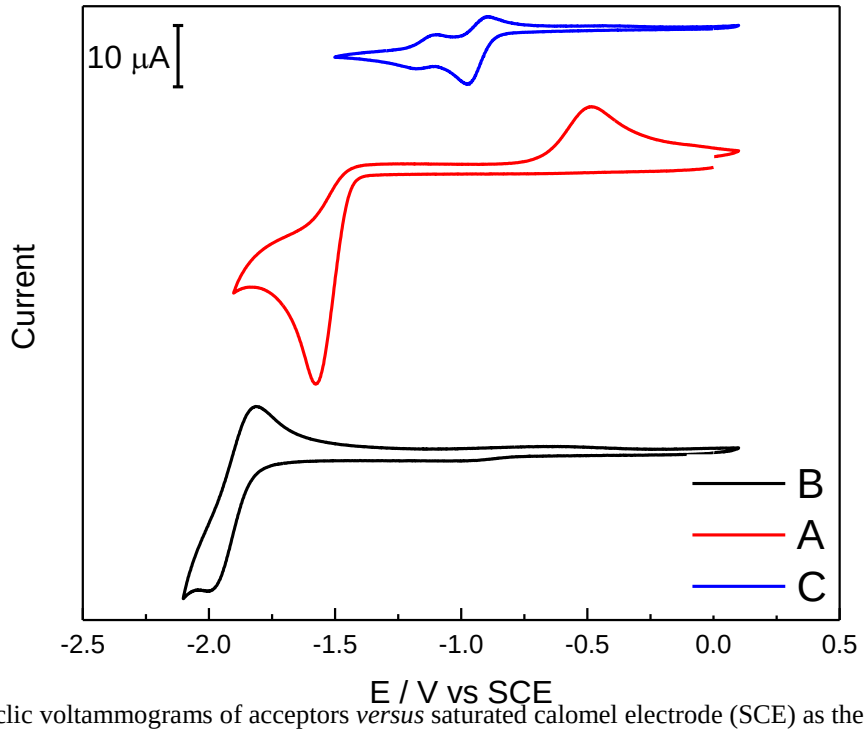

Figure S5. Cyclic voltammograms of acceptors *versus* saturated calomel electrode (SCE) as the reference and 0.2 M Bu_4NPF_6 in CH_2Cl_2 with a scan rate of 200 mV/s.

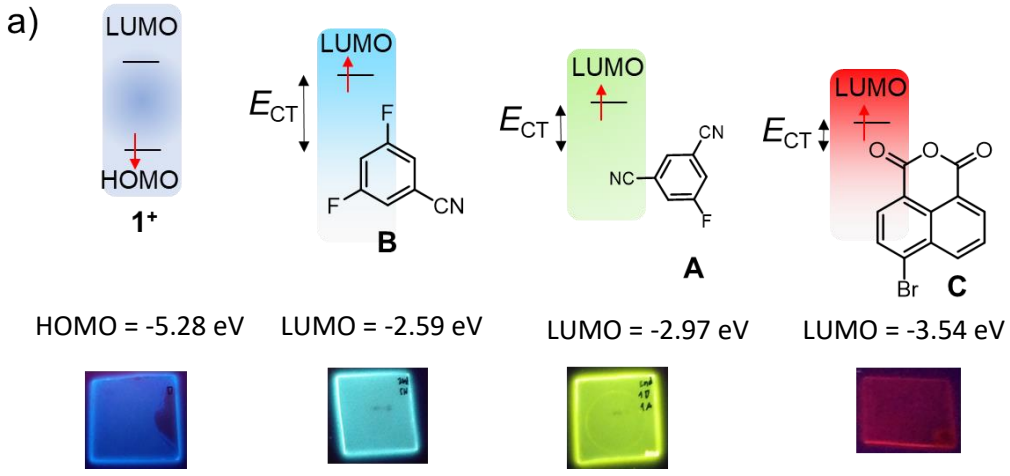

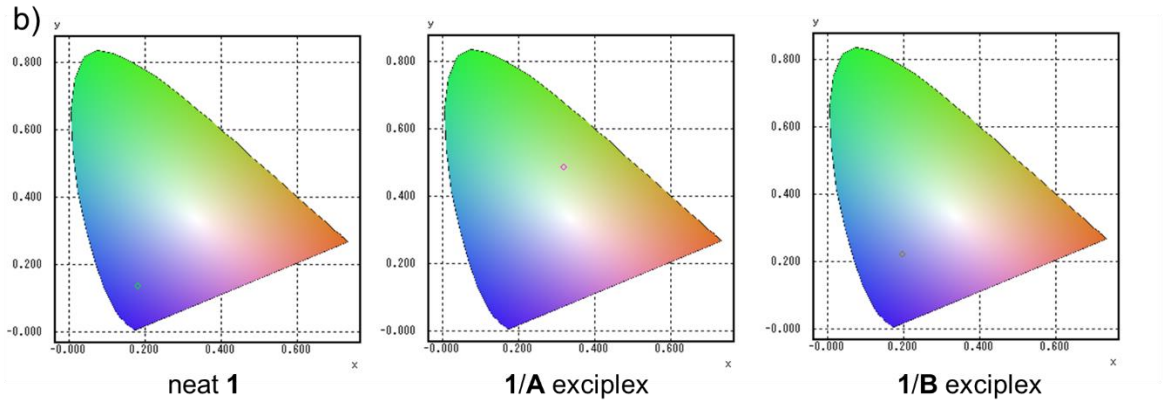

Figure S6. a) Chemical structures of the different electron donor and acceptors screened in this study to obtain multi-colored chiral exciplex luminescence with their HOMO and LUMO values, estimated from their oxidation and reduction potentials (assuming a value of -4.4 eV for 0 V *vs* SCE), and the associated pictures of their film luminescence. We illustrate the various electron excitation steps using the orbitals of the neutral donor/acceptor moieties. Note that dark blue emission on the left corresponds to pure compound **1**. b) CIE diagrams of neat **1**, exciplexes **1**/**B** and **1**/**A** and **1**/**C**, obtained from spin-coated film emissions at 298 K. Note that an accurate CIE diagram for **1**/**C** has not been obtained due to its low photoluminescence quantum yield.

Table S2: Fluorescence quantum yields (Φ) of exciplexes involving **1** and **A**, **B**, or **C** as electron acceptors measured on spin-coated films under air atmosphere.

Compound	**Φ** (%)
1	5.9
1/B	5.6
1/A (1:1, molar ratio)	9
1/A (1:2 molar ratio)	9.3
1/A (2:1 molar ratio)	9.4
1/C	0.6

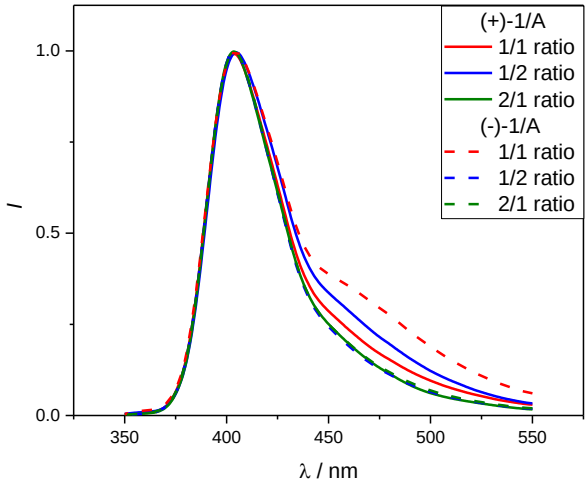

Figure S7. Normalized emission spectra of **1** ((+) or (-) donor) and 5-fluoroisophthalonitrile (A acceptor) mixed in solution with different molar ratio in $CHCl_3$ (*ca.* 10^{-3} M).

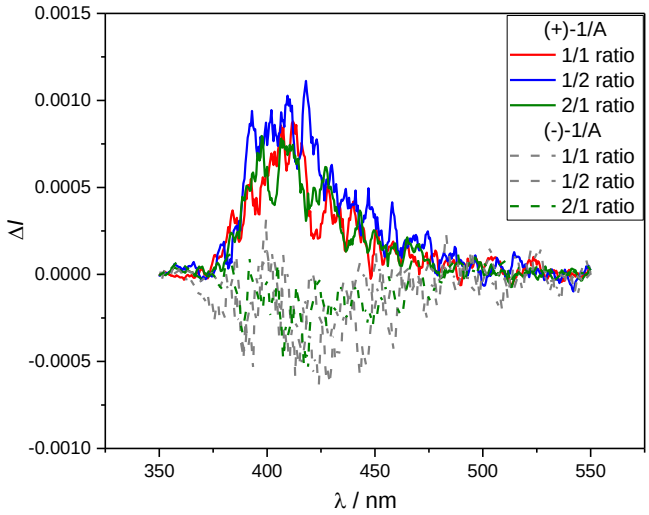

Figure S8. CPL spectra of **1** ((+) or (-) donor) and 5-fluoroisophthalonitrile (A acceptor) mixed in solution with different molar ratio in $CHCl_3$ (*ca.* 10^{-3} M).

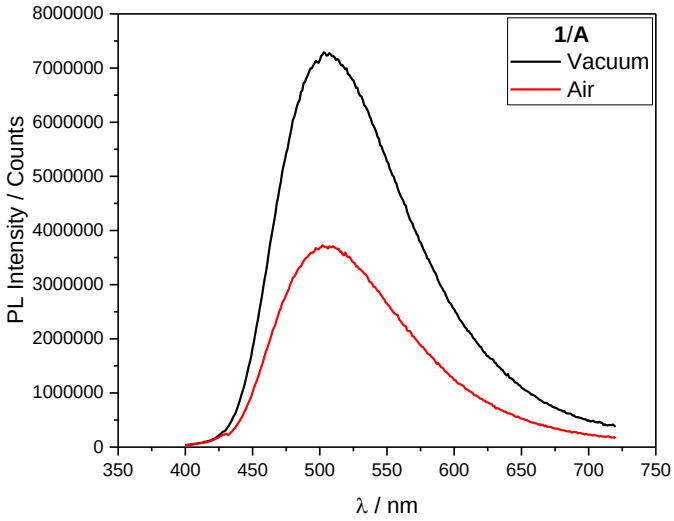

Figure S9. Emission spectra of exciplex in solid state from a spin-coated solution of **1** and 5-fluoroisophthalonitrile (**A** acceptor, ratio 2:1) under vacuum and air.

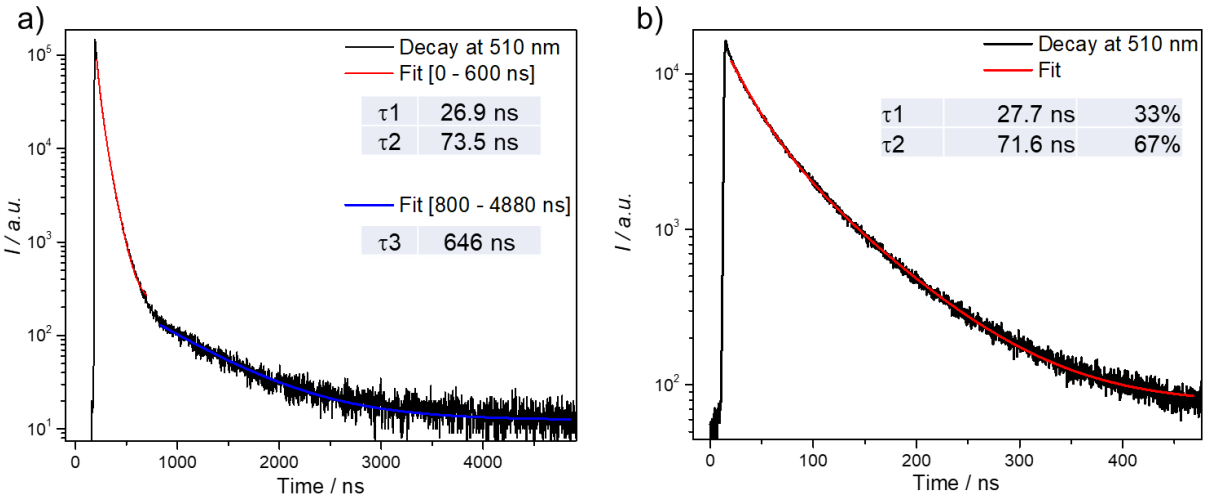

Figure S10. Luminescence decay of exciplex **1** and 5-fluoroisophthalonitrile (**A** acceptor, molar ratio 2:1) in solid state at 298 K and under vacuum (black) with corresponding red and blue fits for the micro- a) and nano-second b) regimes, respectively, monitored at 510 nm.

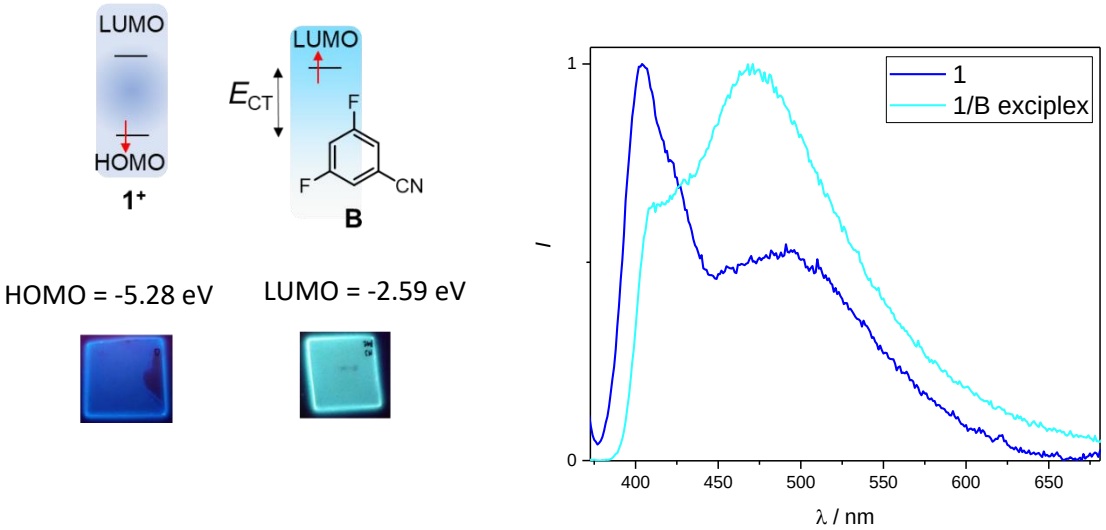

Figure S11. Emission spectra of **1** (blue) and **1**/3,5-difluorobenzonitrile (B) exciplex (sky blue, molar ratio 2:1) with associated pictures.

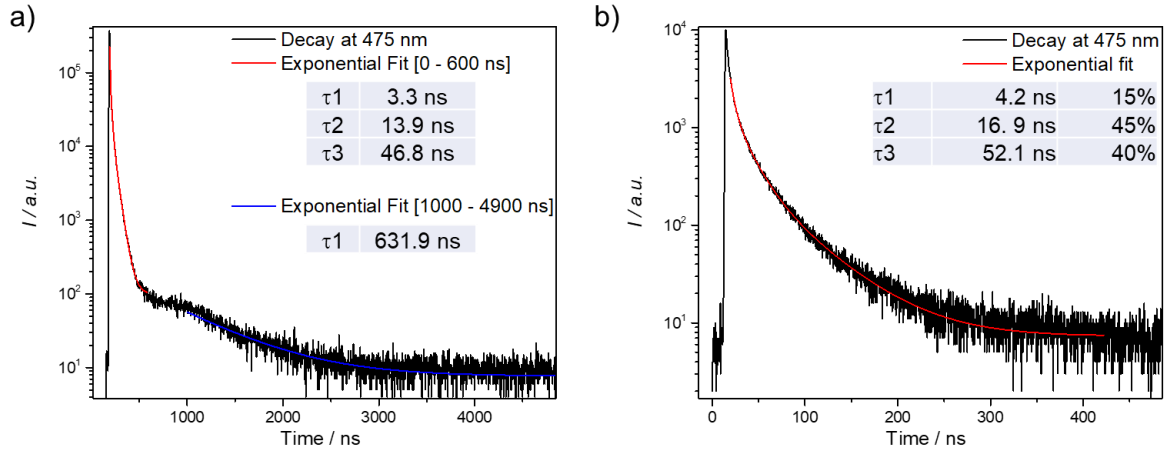

Figure S12. Luminescence decay of exciplex **1** and 3,5-difluorobenzonitrile (**B** acceptor, molar ratio 2:1) in solid state at 298 K and under air (black) with the corresponding blue and red fits in the micro- a) and nano-second b) regimes, respectively, monitored at 475 nm.

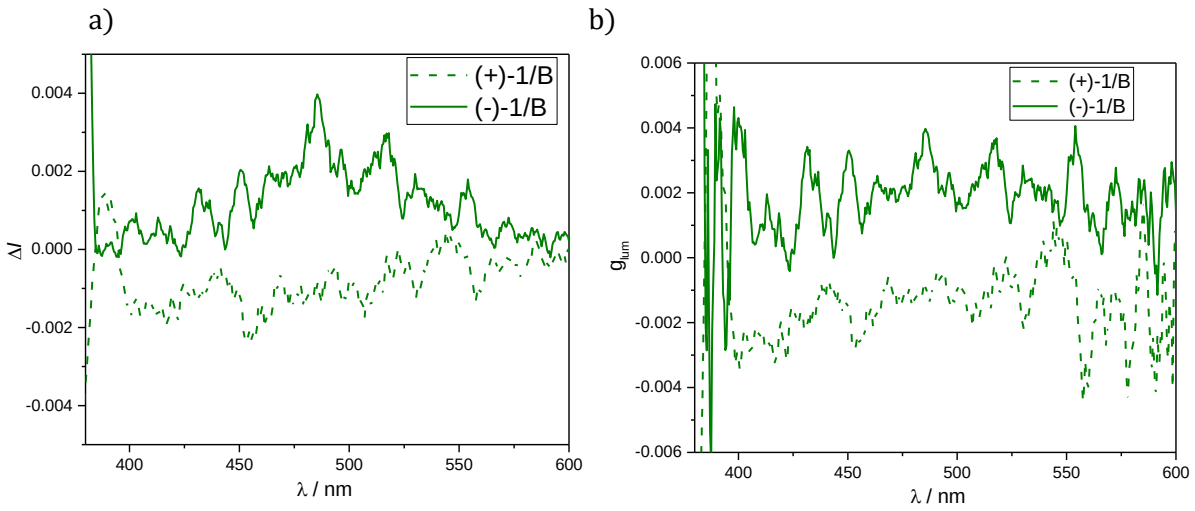

Figure S13. a) CPL spectra and b) g_{lum} factors of exciplex composed of **1** and **B** (3,5 difluorobenzonitrile) measured on spin-coated films at 298 K.

E. Covalent Donor-Acceptor CPL emitter

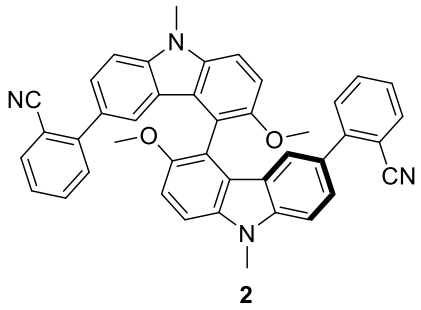

2

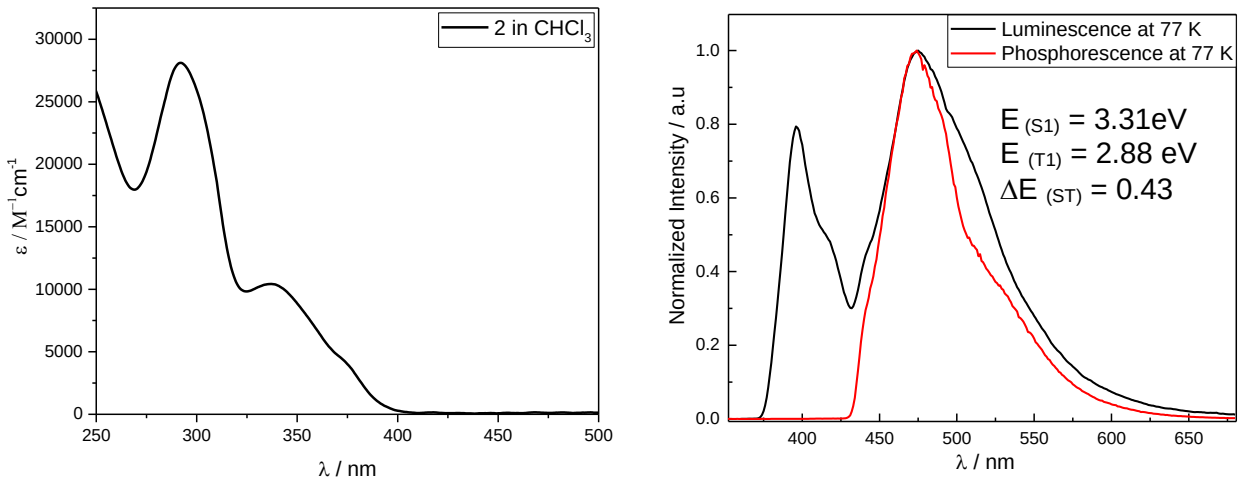

Figure S14. Left: UV-vis spectra of **2** in chloroform (*ca.* 10^{-5} M) at 298 K; right: normalized luminescence spectrum of **2** in 2-methyltetrahydrofuran at 77 K excited at 360 nm (the onset of both fluorescence (F) and phosphorescence (P) emissions are taken to estimate the singlet and triplet energy levels).

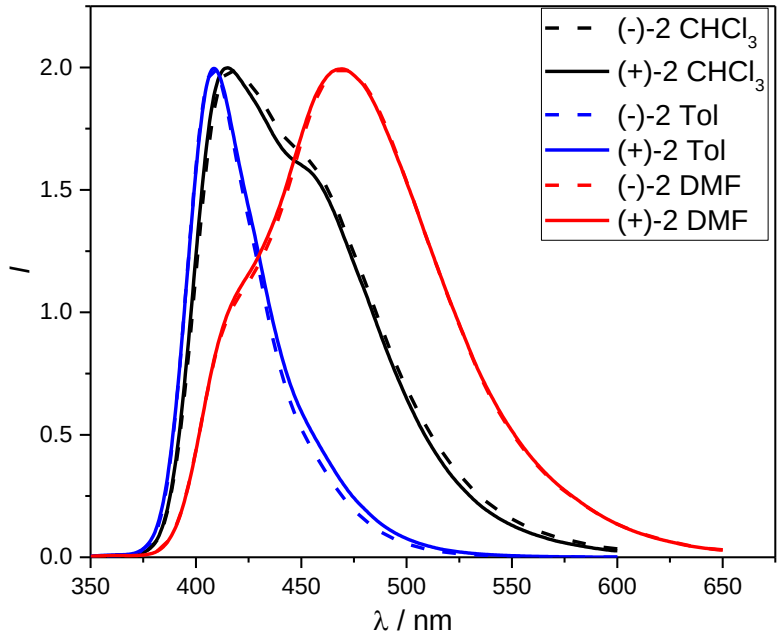

Figure S15. Normalized luminescence spectra of **2** in chloroform (black), toluene (blue) and DMF (red) (*ca.* 10^{-5} M) at 298 K.

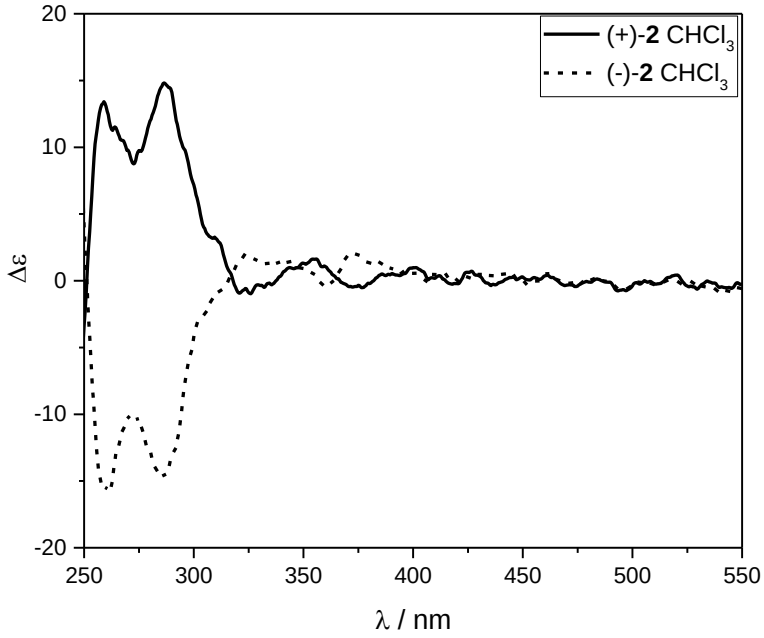

Figure S16. ECD spectra of **2** in chloroform (black) (*ca.* 10^{-5} M) at 298 K.

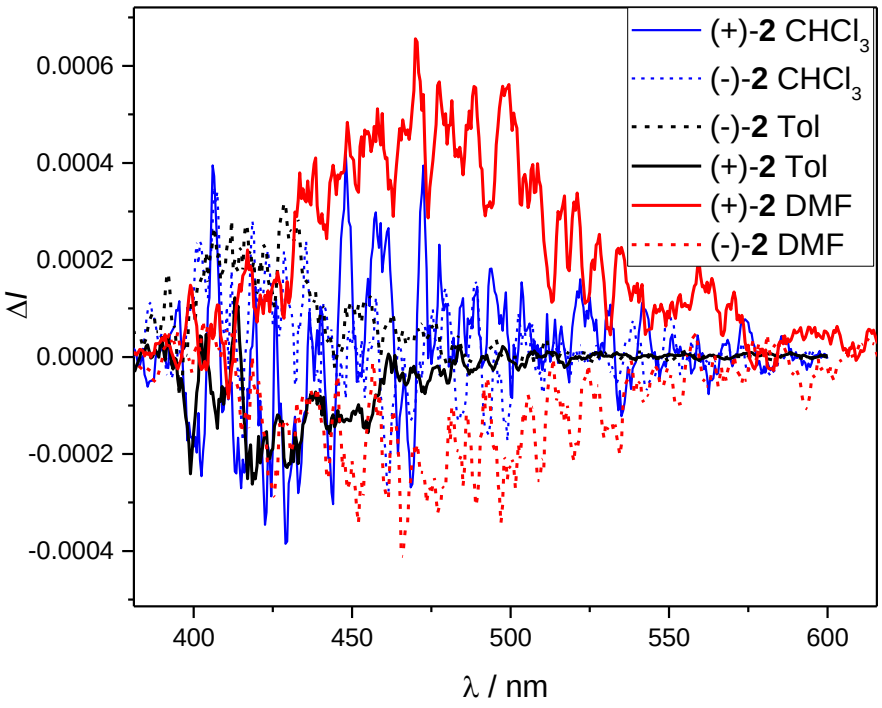

Figure S17. CPL spectra of **2** in $CHCl_3$ (blue), toluene (black) and DMF (red) (*ca.* 10^{-5} M) at 298 K.

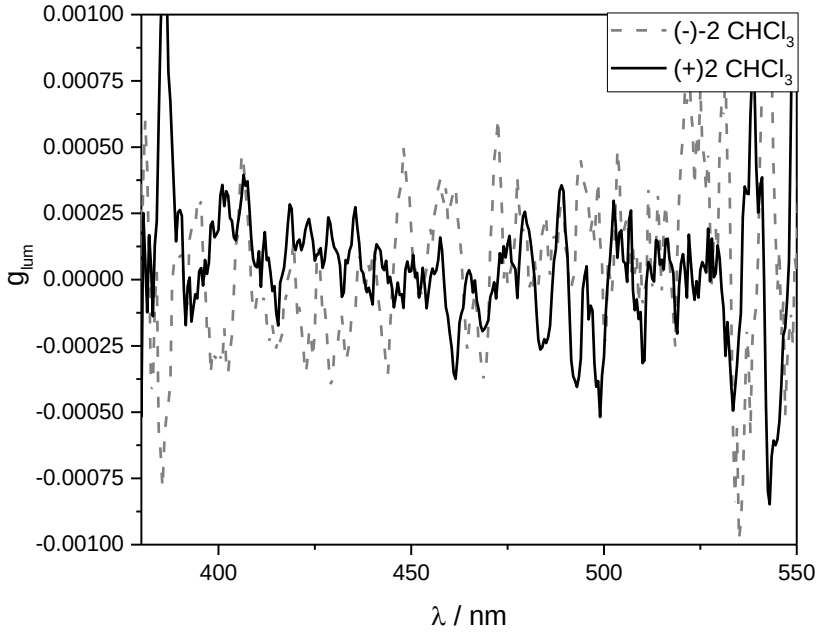

Figure S18. g_{lum} of **2** in $CHCl_3$ (*ca.* 10^{-5} M) at 298 K.

F. X-Ray experimental data

Table S3. X-ray crystallographic data for racemic compound **2**.

Empirical	C42 H30 N4 O2, 3 (CH2Cl2)
CCDC number	2086207
Formula weight	877.48 g/mol
Temperature	150(2) K
Radiation type	Mo-Kalpha
Wavelength	0.71073
Crystal system, space group	triclinic, P -1
Unit cell dimensions	a = 10.7256(12), b = 13.2488(14), c = 16.0772(19),
	alpha = 96.607(4), beta = 100.851(4), gamma = 104.884(4)
Volume	2136.1(4) $Å^3$
Z, Calculated density	2, 1.364 $g.cm^{-3}$
Absorption coefficient	0.445 mm^{-1}
F(000)	904
Crystal size	0.730 x 0.350 x 0.180 mm
Crystal color	colorless
Crystal description	plate
Diffractometer	D8 Venture diffractometer
Theta range for data collection	2.141 to 25.681
(sinTheta/lambda)max (**ล-**1)	0.610
h_min, h_max	-13, 13
k_min, k_max	-16, 16
l_min, l_max	-8, 19
Reflections collected / unique	8041 / 8041 [R(int) = ?]
Reflections [I>2sigma(I)]	6368

Completeness to theta_max	0.993
Absorption correction type	multi-scan
Max. and min. transmission	0.923, 0.774
Refinement method	Full-matrix least-squares on F^2
H-atom treatment	H-atom parameters constrained
Data / restraints / parameters	8041 / 98 / 584
Goodness-of-fit	1.048
Final R indices [I>2sigma(I)]	R1 = 0.1426, wR2 = 0.3665
R indices (all data)	R1 = 0.1636, wR2 = 0.3837
Largest diff. peak and hole	1.865 and -1.459

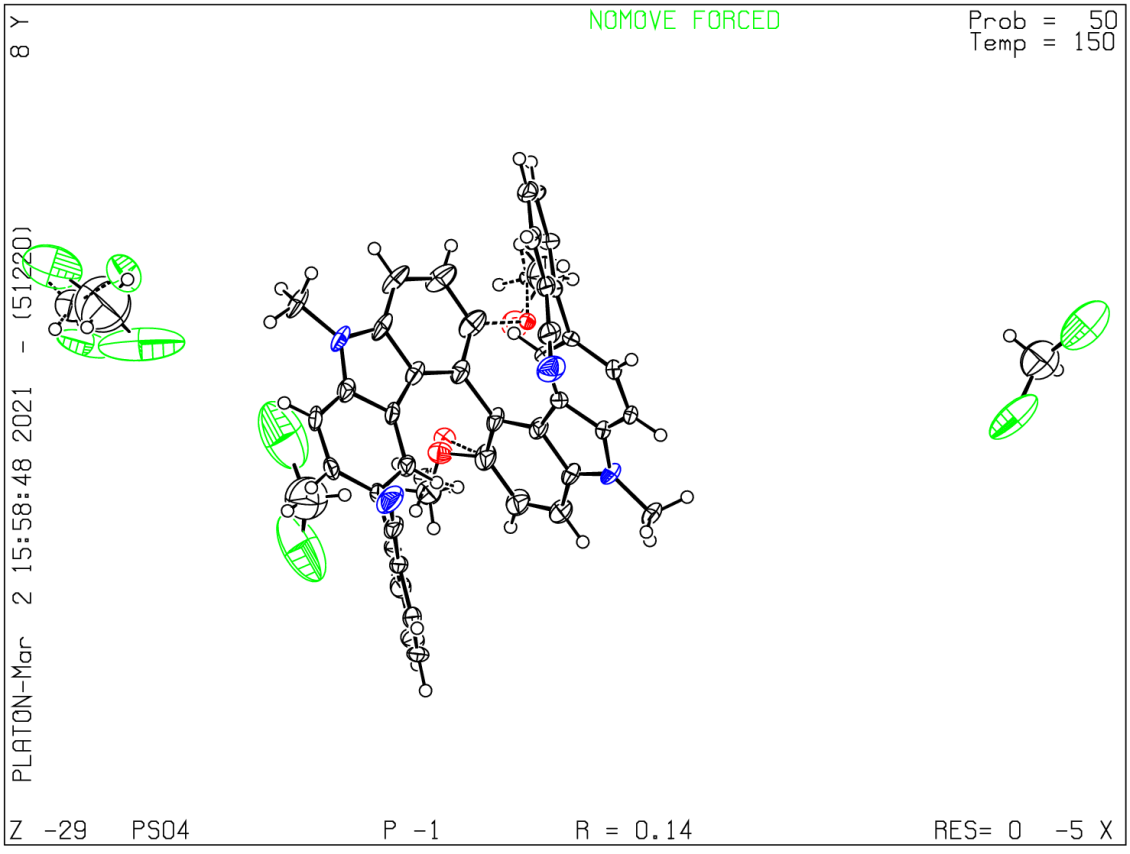

Figure S19. ORTEP diagrams of racemic compound **2** with ellipsoids at 50% probability (at 150 K).

G. SFC separation of the enantiomers of compound 2

Racemate mixture of **2** (20 mg) were dissolved in a minimum amount of DCM (around 500 µL) before injection.

Conditions used for preparative SFC:
Column: Chiralpak IG 250x4.6mm, 5µm; Flow: 4 mL/min; detection: UV at 220 and 290 nm; temperature: 40°C; Co-solvant: CO_2/*i*-PrOH.
Conditions used for the analytical HPLC:
Column: Chiralpak IG 250x4.6mm, 5µm; Flow: 1.5 mL/min; detection: UV at 220 and 290 nm; temperature: 20°C; Solvant: Hexane/*i*-PrOH: 40/60.

Colonne :	CHIRALPAK IG 250 x 4,6 mm, 5µm		
Débit :	1,5 mL/min		
Détection :	220 et 290 nM MaxAbs		
température :	TA		
Solvant :	A : Hexane		
	B : i-PrOH		
Gradient :	Isocratique		
	%A : 40	%B : 60	

Date : 01/04/2021
Opérateur : LEBREQUIER Sabrina
Demandeur : PIETERS Grégory
Encadrant : PIETERS Grégory

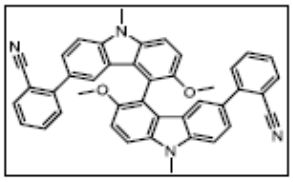

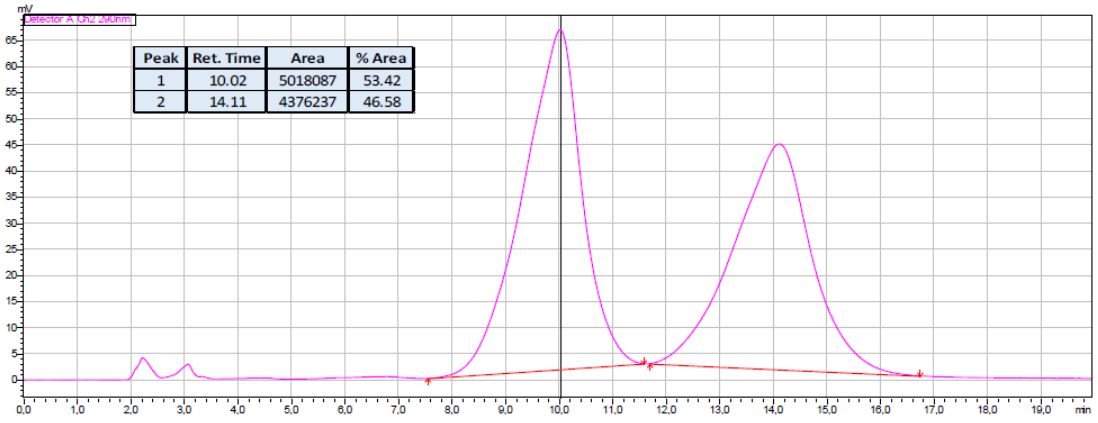

Enantiomer 1

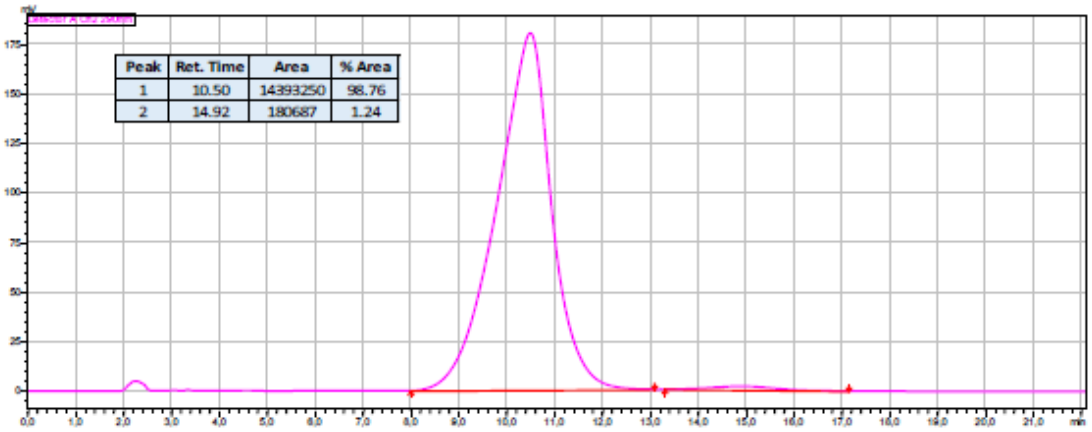

Peak	Ret. Time	Area	% Area
1	10.50	14393250	98.76
2	14.92	180687	1.24

Enantiomer 2

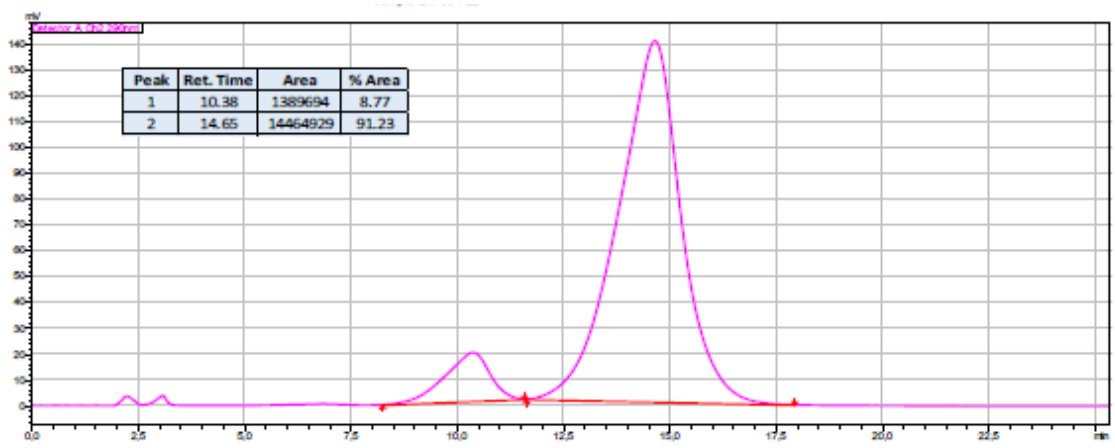

Peak	Ret. Time	Area	% Area
1	10.38	1389694	8.77
2	14.65	14464929	91.23

H. NMR spectra

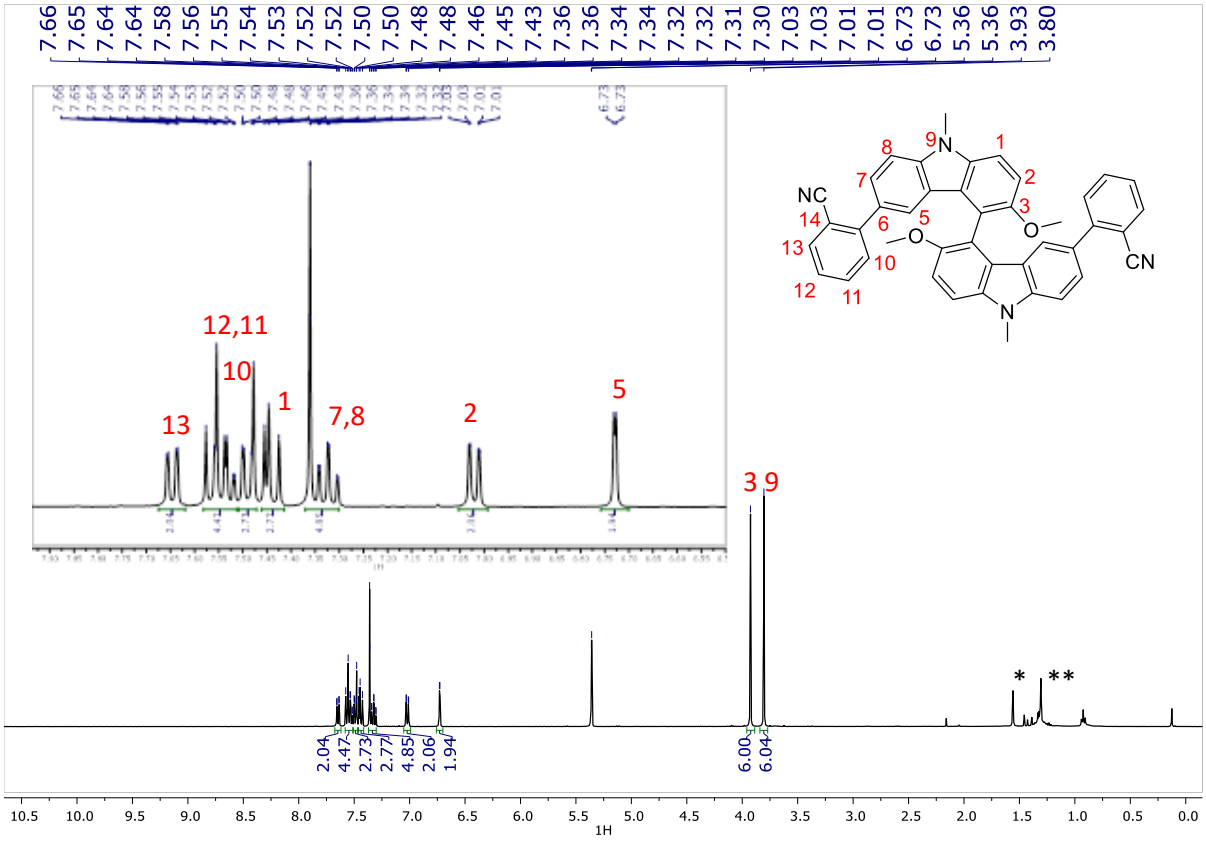

Figure S20. ^{1}H NMR spectrum of **2** in $CDCl_3/CD_2Cl_2$ at 298 K (400 MHz); *denote traces of water and grease.

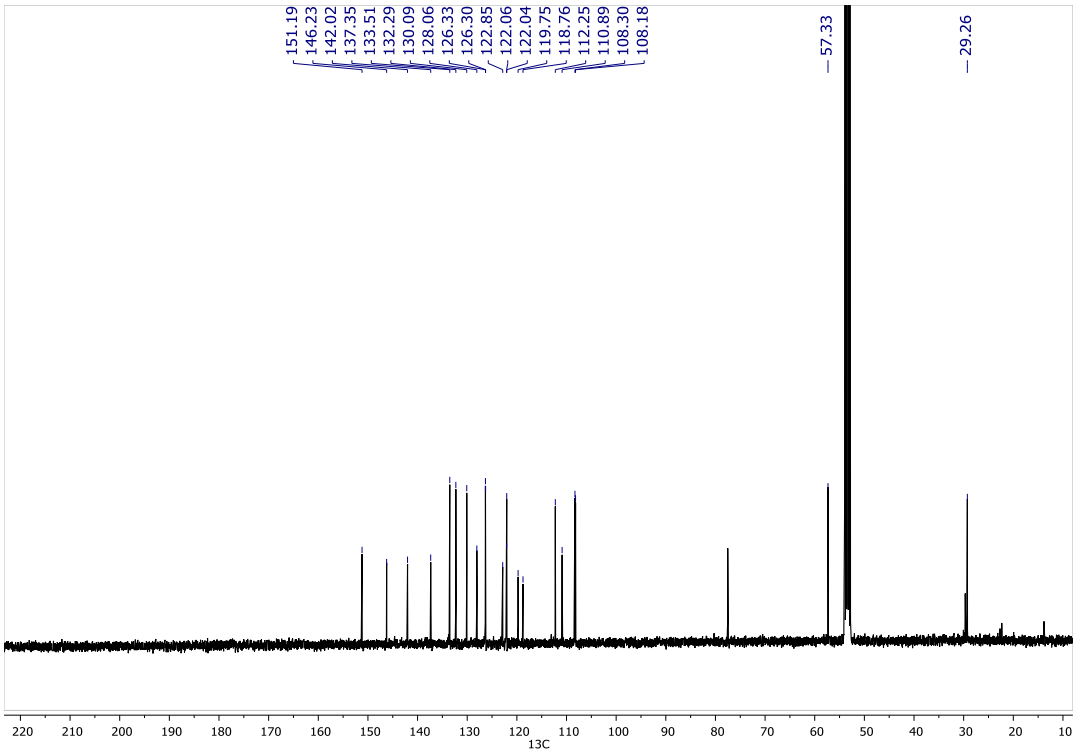

Figure S21. ^{13}C NMR spectrum of **2** in $CDCl_3/CD_2Cl_2$ at 298 K (400 MHz).

I. Theoretical calculations

Computational Details

All computations were performed by using Kohn-Sham Density functional theory (DFT) as implemented in the Gaussian (G16) package,[2] along the PBE0 functional[3] and the def2-SV(P) basis.[4] Solvent effects were included by means of the polarizable continuum model (PCM)[5] for toluene and dimethylformamide (DMF) to match the experimental conditions. Dispersion corrections from Grimme 'D3' were considered in the calculations.[6]

The 200 lowest-energy vertical spin-allowed electronic excitations were calculated for the absorption and electronic circular dichroism (ECD) spectra. In order to simulate the spectral envelopes, the transitions were subsequently Gaussian-broadened with σ = 0.20 eV. For overviews of the theoretical approach to model natural optical activity by quantum chemical calculations, esp. via TD-DFT, see, for example, References [7].[7] Test calculations with B3LYP[8] and CAM-B3LYP[9] functionals for geometry optimizations followed by TD-DFT calculations were performed.
The electronic emission spectra were calculated using the first electronic transition in the excited state optimization in PCM solution for DMF and toluene. Test calculations including the state-specific solvation correction were performed, as well as the CAM-B3LYP functional was also tested.

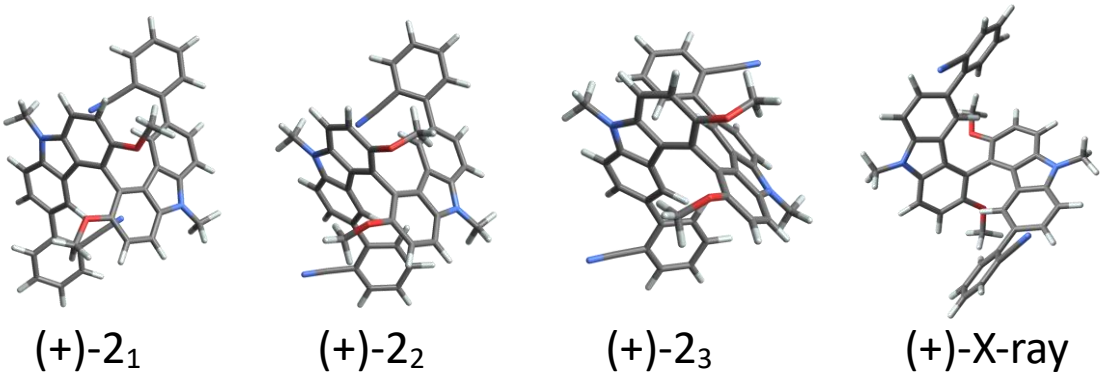

Figure S22. Ground state – DFT optimized geometries for different conformers of **2**.

Table S4. Relative energies (in kcal·mol^{-1}), Boltzmann population ratio at 298 K (in %) and dihedral angle (in degrees) for **2** using PBE0 and CAM-B3LYP functionals.

PBE0	Solvent	Erel (kcal/mol)	Boltzmann population (%)	Dihedral of S_0 (°)
2_1	*DMF*	**0.0**	32.2	83.2
2_2		0.8	8.4	77.3
2_3		0.1	27.2	67.0
X-ray		**0.0**	32.2	107.4
2_1	Toluene	**0.0**	45.0	81.2
2_2		0.9	9.9	76.1
2_3		0.1	38.1	67.6
X-ray		1.1	7.0	110.8
CAM-B3LYP	Solvent	Erel (kcal/mol)	Boltzmann population (%)	Dihedral of S_0 (°)
2_1	DMF	0.0	80.6	82.8
2_2		1.4	7.6	77.6
2_3		1.6	5.4	67.0
X-ray		1.5	6.4	110.7
2_1	Toluene	0.0	86.3	81.6
2_2		1.6	5.8	76.3
2_3		1.5	6.9	69.5
X-ray		2.6	1.1	112.5

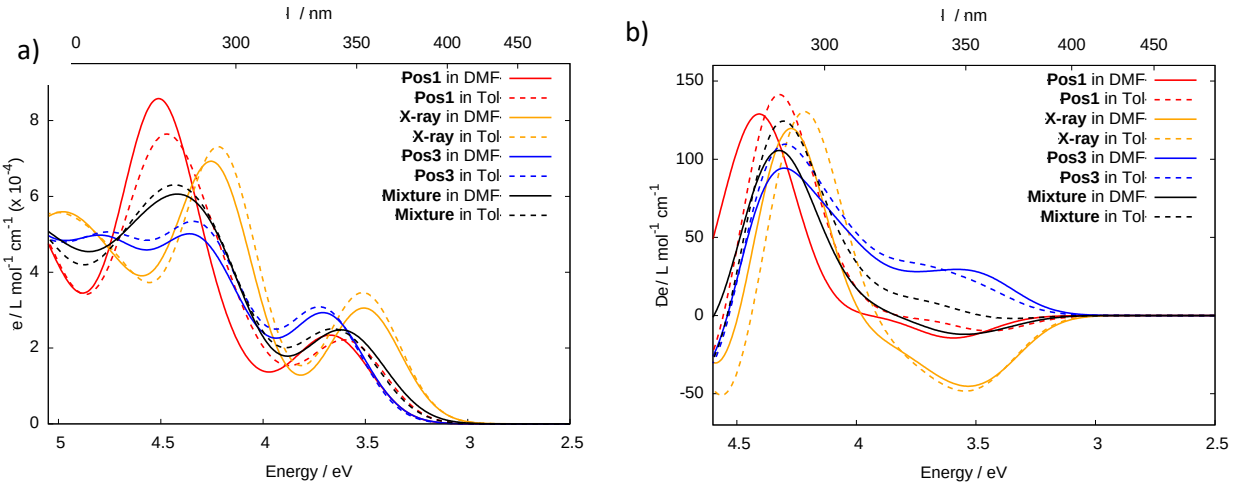

Figure S23. a) Calculated UV/Vis absorption and b) ECD spectra for the different conformers; Pos1 (labelled as $\mathbf{2_1}$ in the text), '**X-ray**' and Pos3 (labelled as $\mathbf{2_3}$ in the text), with DMF and toluene solvents. The calculated spectra labelled as 'mixture' correspond to the Boltzmann average of the three conformers.

Table S5. Selected excitations and occupied (occ)-unoccupied (unocc) MO pair contributions (greater than 10%) for (+)-**2** (**X-ray**) with DMF. H and L indicate the HOMO and LUMO, respectively.

Excitation	**E [eV]**	**λ [nm]**	**f**	**R [10^{-40} cgs]**	**occ. no.**	**unocc no.**	**%**
#1	3.406	364	0.081	73.81	163 (H)	164 (L)	28
					163	166	17
#2	3.473	357	0.090	-310.76	163	165	41
#3	3.530	351	0.268	222.18	163	166	25
					162	165	15
#11	4.172	297	0.087	-471.42	163	169	27
					161	165	11
#12	4.183	296	0.376	385.81	163	168	31
					161	164	10
#15	4.289	289	0.229	440.79	161	166	23
					160	165	17

#17	4.341	286	0.203	299.40	160	165	16
					161	166	15
					161	164	14
#18	4.386	283	0.059	-242.65	160	166	34
#19	4.631	268	0.060	-274.61	161	167	44
#20	4.673	265	0.162	117.24	160	167	32

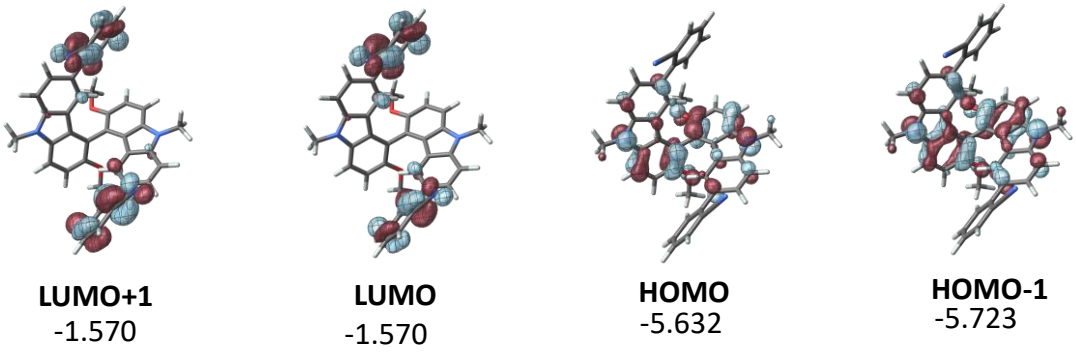

Figure S24. Isosurfaces (±0.035 au) of frontier Molecular Orbitals (MOs) for (+)-**2** (**X-ray, DMF**). Values listed in parentheses are the corresponding orbitals energies in eV.

Table S6. Selected excitations and occupied (occ)-unoccupied (unocc) MO pair contributions (greater than 10%) for (+)-**2** (**2**$_1$) with DMF. H and L indicate the HOMO and LUMO, respectively.

Excitation	**E [eV]**	**λ [nm]**	**f**	**R [10^{-40} cgs]**	**occ. no.**	**unocc no.**	**%**
#1	3.608	344	0.160	403.27	163 (H)	164 (L)	41
#2	3.612	343	0.061	-459.97	163	165	38
#13	4.293	289	0.165	58.56	163	168	23
#17	4.470	277	0.499	867.83	161	166	38
#18	4.537	273	0.131	-316.81	160	166	42
#19	4.547	273	0.252	-724.57	161	167	40
#20	4.595	270	0.335	487.26	160	167	43

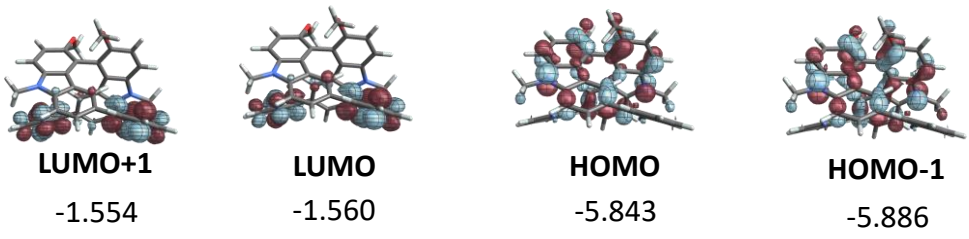

Figure S25. Isosurfaces (±0.035 au) of frontier Molecular Orbitals (MOs) for (+)-**2** (**2**$_1$ in **DMF**). Values listed in parentheses are the corresponding orbitals energies in eV.

Table S8. Relative energies (in kcal·mol^{-1}), Boltzmann population ratio at 298 K (in %), dihedral angle (in degrees), vertical excitation with linear response solvation (in eV, nm in parenthesis) and its oscillator strength for **2** using PBE0 functional.

PBE0	Solvent	Erel	Boltzmann population	Dihedral	Vertical Exc.	Vertical excitation (*f*)
2$_1$	*DMF*	0.0	32.2	83.2	3.608 (344)	0.160
2$_2$		0.8	8.4	77.3	3.596 (345)	0.164
2$_3$		0.1	27.2	67.0	3.537 (351)	0.053
X-ray		0.0	32.2	107.4	3.407 (364)	0.081
2$_1$	Toluene	0.0	45.0	81.2	3.536 (351)	0.052
2$_2$		0.9	9.9	76.1	3.496 (355)	0.008
2$_3$		0.1	38.1	67.6	3.558 (348)	0.055
X-ray		1.1	7.0	110.8	3.416 (363)	0.086

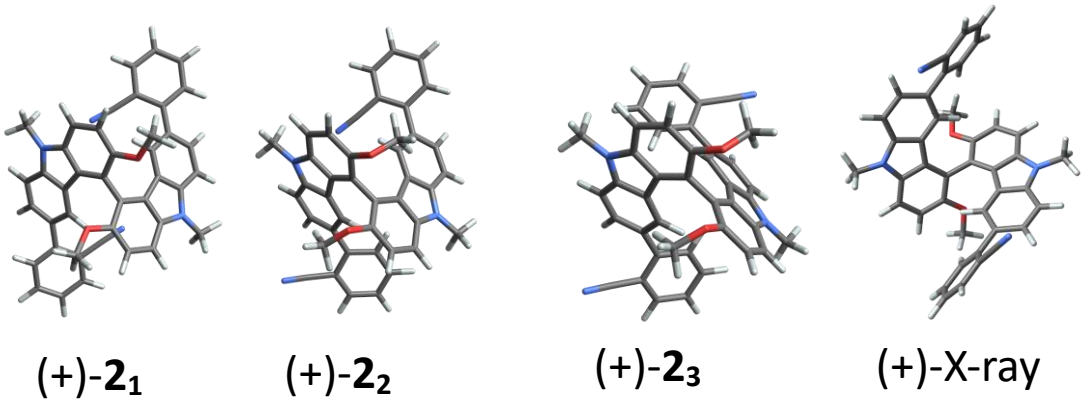

Figure S26. Excited state – DFT optimized geometries for different conformers of **2**. Pos1 is labelled as **2$_1$** in the text.

Table S9. Relative energies (in kcal·mol^{-1}), Boltzmann population ratio at 298 K (in %) and dihedral angle (in degrees) for S_1 of **2** conformers using PBE0 functional.

PBE0	Solvent	Erel (kcal/mol)	Boltzmann population (%)	Dihedral (S_0)
Pos1 (**2$_1$**)	*DMF*	1.3	10.0	107.9
Pos2		*3.7*	0.2	76.1
Pos3		*4.6*	0.0	58.8
X-ray		0.0	89.8	129.7
Pos1 (**2$_1$**)	Toluene	2.0	3.3	87.7
Pos2		5.7	0.0	75.2
Pos3		*4.5*	0.0	67.8
X-ray		0.0	96.7	129.8

Table S10. Relative energy (in kcal·mol^{-1}) for **S$_1$** geometry, Boltzmann population ratio at 298 K (in %), corresponding dihedral angle (θ_d, in degrees), first electronic transition in the excited state optimization in solution (in eV, nm in parenthesis) for the most stable conformers of **2**. Data extracted from the TD-DFT optimization calculation. Values correspond to the $S_1 - S_0$ transition. Also, vertical energy from excited state to ground state emission including state-specific solvation correction (SS-PCM, in eV, nm in parenthesis). It seems that the correction of the solvent does not work for some cases. See Table S11 to see that there are no significant differences between the calculations with and without specific solvation correction.

PBE0	Solvent	Erel	Boltzmann Pop.	θ_d	S_0-S_1	S_0-S_1 (SS-PCM)
2$_1$ (+)-	*DMF*	1.3	10	107.9	2.692 (461)	0.539 (2302)
X-ray (+)-		0.0	90	129.7	2.964 (418)	0.209 (5932)
2$_1$ (+)-	Toluene	2.0	3	87.7	2.704 (459)	1.895 (654)
X-ray (+)-		0.0	97	129.8	3.040 (408)	3.037 (408)

Table S11. Relative energy (in kcal·mol^{-1}) for $\mathbf{S_1}$ geometry, Boltzmann population ratio at 298 K (in %), corresponding dihedral angle (θ_d, in degrees), first electronic transition in the excited state optimization in solution (in eV, nm in parenthesis) for the most stable conformers of **2** using CAM-B3LYP functional. Data extracted from the TD-DFT optimization calculation. Values correspond to the $S_1 - S_0$ transition. Also, vertical energy from excited state to ground state emission including state-specific solvation correction (SS-PCM, in eV, nm in parenthesis) that was included only for comparison between with and without corrections, seeing no significant differences. CAM-B3LYP excitations are shifted and do not agree as well with the experiments as the calculations with the PBE0 functional.

CAM-B3LYP	Solvent	Erel	Boltzmann Pop.	θ_d	S_0-S_1	S_0-S_1 (SS-PCM)
2_1 (+)-	*DMF*	0.0	10	60.1	3.655 (339)	3.672 (338)
X-ray (+)-		0.9	90	131.5	3.303 (375)	3.343 (371)
2_1 (+)-	Toluene	0.0	3	59.9	3.689 (336)	3.699 (335)
X-ray (+)-		1.8	97	131.4	3.391 (366)	3.411 (363)

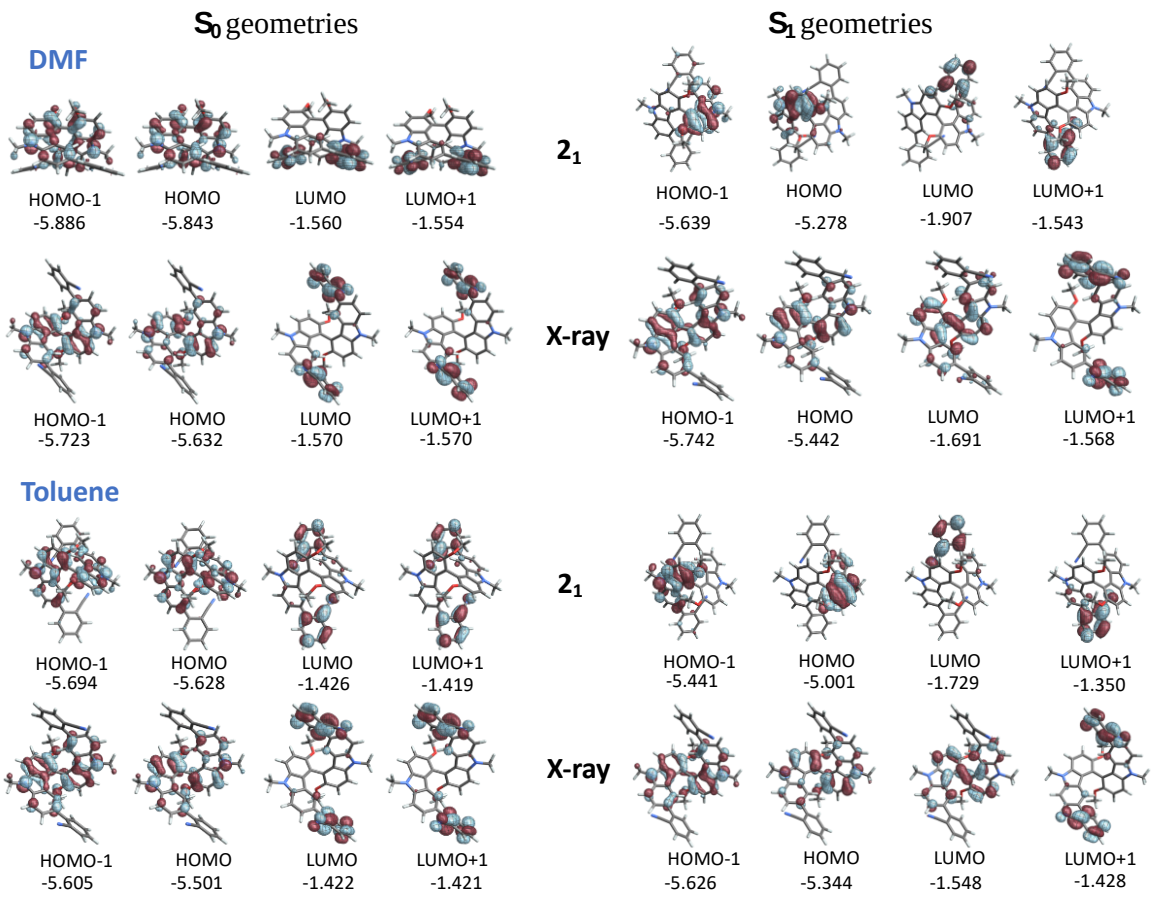

Figure S27. Isosurfaces (±0.035 au) of the frontier molecular orbitals for S_0 and S_1 geometries of **2_1** and X-ray conformers using DMF and toluene solvents. Orbital energies in eV are also plotted.

J. References

[1] Kasemthaveechok, S., Abella, L., Jean, M., Cordier, M., Roisnel, T., Vanthuyne, N., Guizouarn, T., Cador, O., Autschbach, J., Crassous, J., Favereau, L., Axially and Helically Chiral Cationic Radical Bicarbazoles: SOMO-HOMO Level Inversion and Chirality Impact on the Stability of Mono- and Diradical Cations, *J. Am. Chem. Soc.* **2020**, *142*, 20409-20418.

[2] M. J. Frisch, G. W. T., H. B. Schlegel, G. E. Scuseria, , M. A. Robb, J. R. C., G. Scalmani, V. Barone, , G. A. Petersson, H. N., X. Li, M. Caricato, A. V. Marenich, , J. Bloino, B. G. J., R. Gomperts, B. Mennucci, H. P. Hratchian, , J. V. Ortiz, A. F. I., J. L. Sonnenberg, D. Williams-Young, , F. Ding, F. L., F. Egidi, J. Goings, B. Peng, A. Petrone, , T. Henderson, D. R., V. G. Zakrzewski, J. Gao, N. Rega, , G. Zheng, W. L., M. Hada, M. Ehara, K. Toyota, R. Fukuda, , J. Hasegawa, M. I., T. Nakajima, Y. Honda, O. Kitao, H. Nakai, , T. Vreven, K. T., J. A. Montgomery, Jr., J. E. Peralta, , F. Ogliaro, M. J. B., J. J. Heyd, E. N. Brothers, K. N. Kudin, , V. N. Staroverov, T. A. K., R. Kobayashi, J. Normand, , K. Raghavachari, A. P. R., J. C. Burant, S. S. Iyengar, , J. Tomasi, M. C., J. M. Millam, M. Klene, C. Adamo, R. Cammi, , J. W. Ochterski, R. L. M., K. Morokuma, O. Farkas, , J. B. Foresman, D. J. F., Gaussian, Inc., Wallingford CT, **2016. URL: www.gaussian.com.**

[3] Adamo, C., Barone, V., Toward reliable density functional methods without adjustable parameters: The PBE0 model, *J. Chem. Phys.* **1999**, *110*, 6158-6170.

[4] aWeigend, F., Ahlrichs, R., Balanced basis sets of split valence, triple zeta valence and quadruple zeta valence quality for H to Rn: Design and assessment of accuracy, *Phys. Chem. Chem. Phys.* **2005**, *7*, 3297-3305; bWeigend, F., Accurate Coulomb-fitting basis sets for H to Rn, *Phys. Chem. Chem. Phys.* **2006**, *8*, 1057-1065.

[5] Scalmani, G., Frisch, M. J., Continuous surface charge polarizable continuum models of solvation. I. General formalism, *J. Chem. Phys.* **2010**, *132*, 114110.

[6] Grimme, S., Antony, J., Ehrlich, S., Krieg, H., A consistent and accurate ab initio parametrization of density functional dispersion correction (DFT-D) for the 94 elements H-Pu, *J. Chem. Phys.* **2010**, *132*, 154104.

[7] aAutschbach, J., Nitsch-Velasquez, L., Rudolph, M., Time-dependent density functional response theory for electronic chiroptical properties of chiral molecules, *Top. Curr. Chem.* **2011**, *298*, 1-98; bSrebro-Hooper, M., Autschbach, J., Calculating Natural Optical Activity of Molecules from First Principles, *Annu. Rev. Phys. Chem.* **2017**, *68*, 399-420.

[8] Becke, A. D., Density-functional thermochemistry. III. The role of exact exchange, *J. Chem. Phys.* **1993**, *98*, 5648-5652.

[9] Yanai, T., Tew, D. P., Handy, N. C., A new hybrid exchange–correlation functional using the Coulomb-attenuating method (CAM-B3LYP), *Chem. Phys. Lett.* **2004**, *393*, 51-57.